Nonlinear Ferromagnetic Resonance and Foldover in Yttrium Iron Garnet Thin Films—Inadequacy of the Classical Model

Yuri K. Fetisov, *Senior Member, IEEE,* Carl E. Patton, *Fellow, IEEE,* and Valeri T. Synogach

***Abstract*— A thin-film resonator structure has been used for quantitative measurements of ferromagnetic resonance foldover and the associated bistable power response for yttrium iron garnet (YIG) thin films. The resonator consisted of a 1-mm by 1-mm-square, 4.9-μm-thick epitaxial YIG film on top of a 50-μm-wide, 3-mm-long microstrip transducer. A static magnetic field of 3200 Oe was applied perpendicular to the film. Low-order magnetostatic forward volume wave standing modes were excited at low power levels in the -20-dBm range and detected as resonance dips in reflected power versus frequency spectra over the range 4–5 GHz. At powers in the 0- to $+15$-dBm range, these dips showed foldover and bistable response characteristics for increasing and decreasing frequency or power sweeps. The use of 1–10-μs-wide pulses instead of continuous-wave (CW) excitation resulted in the consistent disappearance of the foldover and bistability characteristics. The frequency sweep pulse data at fixed power reproduced the down-sweep CW results, and the pulse data for both increasing and decreasing power at fixed frequency reproduced the increasing-power CW results. A quantitative theoretical analysis demonstrates that observed foldover and bistable response characteristics are much weaker than predicted from the classical precession foldover mechanism proposed by Anderson and Suhl, in which the decrease in the static component of the magnetization drives the response. The up-sweep and down-sweep foldover frequency jumps both occur sooner than predicted by this classical mechanism and the calculated foldover profiles are much more severe than the data show.**

***Index Terms*— Magnetic films, magnetic resonance, magnetostatic waves, magnetostatic volume waves.**

I. Introduction

BISTABLE phenomena based on the interaction of electromagnetic radiation with different nonlinear resonance systems are of interest for both the basic elucidation of nonlinear effects and for device applications. Most studies in this area have been carried out in the optical regime with the aim to elaborate optically controlled bistable devices for application in optical computers [1]. The simplest passive optical bistable system is an optical resonator containing a nonlinear material with a refraction or absorption coefficient which depends on the light intensity. A suitably designed resonator would have a hysteretic power response with two different levels of transmitted or reflected light over some suitable range of input power.

Under suitable conditions, ferromagnetic resonance (FMR) and the closely related magnetostatic wave (MSW) resonances in magnetic films offer the possibility of a similar bistable response in the microwave frequency regime. These microwave resonances can be set up to satisfy the two conditions which are needed for bistability: 1) a transmission or reflection coefficient which depends on the signal frequency and 2) some kind of feedback response such as a power dependent resonance frequency or absorption coefficient.

These power dependent microwave effects in magnetic films are closely related to so-called "foldover" phenomena in ferromagnetic resonance. Foldover in the FMR response at high power levels was first proposed by Anderson and Suhl [2] for perpendicularly magnetized magnetic films or slabs. The basic effect is a bistable absorption curve which depends on the direction of the frequency or magnetic field sweep. The bistable response is driven by the change in the static component of the precessing magnetization with either frequency or power. This change shifts the FMR frequency and produces a bistable response. The term "foldover" derives from the schematic form of the FMR response at high power first depicted by Weiss [3].

Two schematic foldover FMR response curves are shown in Fig. 1. Both diagrams show absorbed power P_a as a function of frequency f for the FMR response. The diagram in Fig. 1(a) shows the multivalued FMR response which is obtained for an FMR frequency which increases with the power absorption. The diagram in Fig. 1(b) shows the corresponding power absorption versus frequency profile which would be found experimentally. Data which resemble the profile in Fig. 1(b) will be presented in Section III. The details of the classical FMR response analysis which leads to such curves will be considered in Section IV.

Following the initial prediction of foldover in [2] and the first experimental report of foldover by Weiss [3], a number of authors have published results on foldover effects due to spin wave instability, magnetocrystalline anisotropy, and sample heating [4]–[16]. However, as aptly pointed out by Seagle

Manuscript received May 28, 1999. This work was supported in part by the National Science Foundation under Grant DMR-9801649, the U.S. Army Research Office by Grants DAAH04-95-1-0325 and DAAG55-98-1-0430, and the Office of Naval Research by Grant N00014-94-1-0096.

Y. K. Fetisov is with the Moscow Institute of Radio Engineering, Electronics, and Automation (MIREA), Moscow, 117454 Russia.

C. E. Patton is with the Department of Physics, Colorado State University, Fort Collins, CO 80523 USA (e-mail: patton@lamar.colostate.edu).

V. T. Synogach is with the Department of Physics, Colorado State University, Fort Collins, CO 80523 USA, on leave from the Institute of Solid State Physics, Russian Academy of Sciences, Chernogolovka 142432, Moscow District, Russia.

Publisher Item Identifier S 0018-9464(99)09378-4.

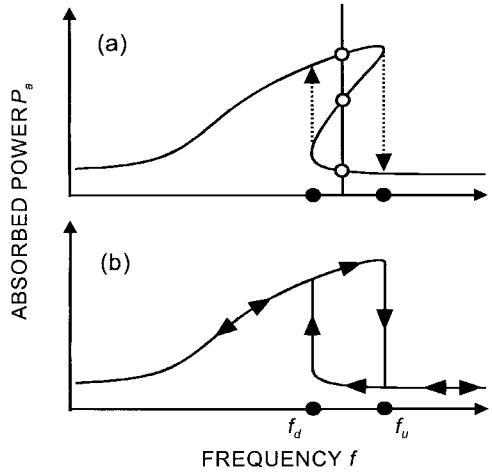

Fig. 1. Schematic high power ferromagnetic resonance curves of absorbed power P_a versus frequency f under conditions which produce a foldover response. Diagram (a) shows the multivalued FMR profile and the foldover character. Diagram (b) shows the corresponding profile which would be realized experimentally, with the up-sweep jump J_u at frequency f_u, and the down-sweep jump J_d at frequency f_d, as indicated.

et al. [10], "no clear evidence of this effect (*sic* the classical foldover effect of [2]) has been produced." The authors of [10] also point out, quite correctly, that "Problems resulting from spin wave instabilities and thermal effects have left vague the interpretation of experiments."

The purpose of this paper is to describe new results on foldover and bistability observed through the nonlinear response of a microstrip transmission line coupled to a single crystal yttrium iron garnet (YIG) thin film which is biased close to ferromagnetic resonance. These new results contribute to the ongoing saga of ferromagnetic resonance foldover in several ways. First, the use of a nonresonant microstrip line and a resonator structure with a small area (111) YIG film avoids the problems of magnetocrystalline anisotropy, sample heating, and high Q cavity interactions which have complicated some of the work cited above. Second, the use of a perpendicular geometry, with the film magnetized perpendicular to the film plane, eliminates the possibility of degenerate spin waves and parametric spin wave processes which have complicated some of the work cited above. Third, careful measurements of the jump frequencies and power levels associated with the observed foldover make possible quantitative comparisons with the Anderson–Suhl model. Fourth, measurements under pulsed as well as CW excitation conditions provide a further check on the influence of heating effects on the observed foldover profiles.

The necessary frequency selective absorption associated with the FMR or MSW excitations in high quality YIG films is manifested by extremely sharp resonances with widths in the one MHz range and absorption coefficients which can approach unity. Moreover, the change in the FMR frequency and the absorption with power have been studied extensively in YIG disks [3], YIG spheres [9], and thin YIG films [10], [11], [13], [14]. Of direct relevance to the present work are the measurements of an explicit microwave power dependent shift in the frequency of thin YIG film MSW resonators by 2–25 MHz at powers up to several watts [17], [18], as well as the observation of a nonlinear dependence of MSW propagation losses on power [19].

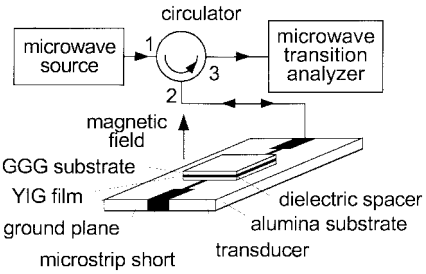

Fig. 2. Schematic view of a thin film YIG resonator structure and the microwave measurement system.

Technical bistable device effects in the microwave regime have also been considered explicitly. Recent work includes a theoretical analysis of the bistable response characteristics of magnetostatic surface wave (MSSW) YIG film resonators with distributed feedback [20], an experimental study of bistability for an MSW oscillator with a nonlinear MSSW element in the feedback circuit [21], and an MSSW interferometer with external magnetic field feedback [22].

The above device effects aside, the present investigation represents the first fundamental investigation of FMR foldover and bistability based on a simple microstrip MSW resonator structure. Section II describes the thin film YIG resonator and the experimental setup used for the foldover and bistability experiments. Section III presents the experimental results. Section IV summarizes the theoretical analysis based on the Anderson–Suhl model and presents comparisons of the measured frequency and power jump points from the foldover data with theory. Section V gives comments on possible applications.

II. The Experiment

Fig. 2 shows the schematic view of the thin film YIG resonator used in the experiments and a block diagram of the measurement system. The basic element of the resonator was a (111) single crystal 4.9 μm thick YIG film grown by liquid-phase-epitaxy method on a 0.5 mm thick gallium-gadolinium-garnet (GGG) substrate. The actual resonator element was a 1 mm $\times$ 1 mm square which was cut from the as grown film. The film square was centered on top of a narrow microstrip transducer section, and was separated from the microstrip by a 100 μm thick dielectric spacer, as indicated. This spacer served to decrease the coupling between the microstrip line and the YIG film. Some data were also obtained on a 4 mm $\times$ 1 mm 25 μm thick film.

The microstrip circuit in Fig. 2 was fabricated from a 0.5 mm thick alumina support slab which was metallized on the back side. The circuit was evaporated on the top side of the alumina. The microstrip transducer under the YIG element was 50 μm wide and 3 mm long. This line was connected to standard 50 Ω microstrip sections, one shorted to the microstrip ground plane and the other connected to the microwave source and the microwave transition analyzer

through a circulator. The entire structure was placed between the poles of a permanent magnet to provide a nominally uniform static external magnetic field of 3200 Oe directed perpendicular to the plane of the YIG film and the microstrip structure. This configuration corresponds to a rejection filter arrangement such that the reflected power shows a drop at ferromagnetic resonance. A Hewlett Packard model 83 650A synthesized sweeper was used as a source for CW or pulsed microwave power at 4–5 GHz and power levels up to +20 dBm. The microwave signal reflected from the resonator was processed with a Hewlett Packard model 70 820A microwave transition analyzer. All data were collected and analyzed through a personal computer.

The system in Fig. 2 was used in two measurement modes. First, the reflected power from the resonator was measured versus frequency for both increasing and decreasing frequency scans at various fixed microwave power levels. Second, the resonator response was measured as a function of increasing or decreasing power at fixed frequency. Both series of measurements were made with both CW and pulse microwave excitation. The pulse measurements were made for pulse widths of 1–10 μs at a pulse repetition period of 1 ms.

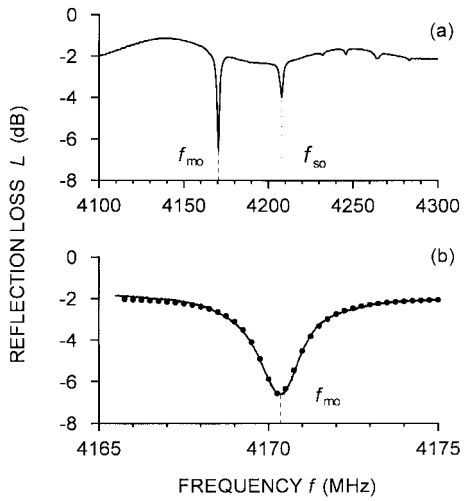

Fig. 3. Reflection loss L, in dB, as a function of frequency f for the YIG resonator structure at a CW input power of -20 dBm. The solid curve in graph (a) shows the main resonance absorption dip centered at $f_{mo} = 4170.3$ MHz, a second strong peak at $f_{so} = 4207.8$ MHz, and a number of smaller modes at higher frequencies. The solid line in graph (b) shows the f_{mo} resonance on an expanded scale. The solid points in (b) show a fitted Lorentzian absorption response.

III. Experimental Results

A. Low Power Response

The CW low power frequency response characteristics of the YIG resonator are shown in Fig. 3. The input power to the resonator element for the data shown was -20 dBm. The solid curves in both graphs show the reflection loss L of the structure, expressed in dB, as a function of the frequency f. The 200 MHz scale of the graph in Fig. 3(a) is sufficient to show the main resonance absorption dip centered at $f_{mo} = 4170.3$ MHz, a second strong peak at $f_{so} = 4207.8$ MHz, and a number of smaller modes at higher frequencies. These modes are related to the various standing wave resonances excited in the 1 mm square YIG film element. The graph in Fig. 3(b) shows the main resonance dip on an expanded scale. The solid points show a fitted Lorentzian response. The fit will serve as a basis for the classical foldover analysis in Section IV. The profiles shown in Fig. 3 are typical of the low power response. Similar profiles were found for input power levels from -60 up to -20 dBm.

The resonances shown in Fig. 3 are associated with the microstrip excitation of magnetostatic forward volume wave (MSFVW) modes [23] in the YIG film. If one assumes a fully pinned dynamic magnetization at the film edges, one may write the standing mode in-plane wave numbers for the allowed MSFVW resonances as

$$k_{n,l} = \frac{\pi}{a}\sqrt{n^2 + l^2} \tag{1}$$

where a is the side length for the square film and n and l are integers. For the excitation geometry in Fig. 2, one may assume that the MSFVW modes which are strongly excited correspond only to odd integer values for n and l. Modes with an even number of half wavelengths cross the film direction perpendicular to the microstrip line, corresponding to $l = 2,\ 4$, etc., have odd symmetry relative to the symmetric microwave field produced by the microstrip and would not be strongly excited.

One would expect to find strongest coupling for $n = 1$ and $l = 1$, which corresponds to a standing mode with a half wavelength across each side of the film. This mode is identified as the f_{mo} dip in Fig. 3. One might also expect to see a slightly weaker mode for $n = 1$ and $l = 3$, which corresponds to a standing mode with a three half wavelengths across the side of the film. This mode is identified as the f_{so} dip in Fig. 3.

The MSFVW standing mode frequencies may be obtained from (1) and the lowest order branch of the frequency versus wave number dispersion relation for MSFVW excitations. The wave numbers from (1) for low value n and l indices are on the order of 40–100 rad/cm and the corresponding $k_{n,l}d$ products, where d is the film thickness, are well below unity. In the $k_{n,l}d \ll 1$ limit, one may write the MSFVW dispersion equation in the form

$$\frac{f_{n,l}^{(o)}}{|\gamma|} = (H_{ext} + H_{adj} - 4\pi M_s) + 4\pi M_s\left(\frac{2d}{a} + \frac{dk_{n,l}}{4}\right). \tag{2}$$

In (2) $f_{n,l}^{(o)}$ denotes the frequency of the (n, l) mode in the limit of low power. $|\gamma|$ is the absolute value of the YIG gyromagnetic ratio, taken to have the nominal free electron value of 2.8 MHz/Oe, H_{ext} is the applied external static magnetic field, H_{adj} is a small adjustment field to account for anisotropy, etc., and $4\pi M_s$ is the saturation induction. The nominal value of $4\pi M_s$ for YIG is 1750 G.

The first term on the right-hand side of (2) corresponds to the usual uniform mode ferromagnetic resonance frequency for a perpendicularly magnetized thin film in the large area

limit. The $2d/a$ term represents the first order demagnetizing factor correction for a film of thickness d and lateral size a [24]. The $dk/4$ term is the k-dependent MSFVW dispersion term to lowest order.

Based on the numerical values for the experimental and material parameters given above, the frequency $f_{1,1}^{(o)}$ from (2) may be matched to the observed f_{mo} resonance peak at 4170.3 MHz with an adjustment H_{adj} value of +12.7 Oe. An H_{adj} value in the 10 Oe range is reasonable to take into account small deviations of γ and $4\pi M$ from the nominal values cited above, small errors in the measured value of the static field and the nominal film thickness, etc., as well as small anisotropy effects. Precise determinations of these effects are not needed for the present study, and H_{adj} is used here simply to match the calculated mode position to experiment and serve as a check on the mode identification. These same numerical data yield a calculated $f_{1,3}^{(o)}$ of 4203.3 MHz. This is reasonable agreement with the observed f_{so} point at 4207.8 MHz. The spacing of the $f_{1,1}^{(o)}$ and the $f_{1,3}^{(o)}$ modes would also be affected by deviations in the magnetization, film thickness, and lateral film dimensions from the nominal values cited above, so the match here may also be considered to be adequate. The focus of this study was on the high power response of the main resonance at f_{mo}.

B. High Power Response

For CW input microwave powers higher than -20 dBm or so, the resonator response became power dependent. Fig. 4 shows a typical series of response curves of the reflection loss L versus frequency f for values of the input power $P_{\rm in}$ from -20 dBm up to $+10$ dBm. The data shown are for CW microwave excitation at a slow frequency sweep rate of 20 MHz/s. This rate was low enough to avoid transient effects. The data shown were obtained in 1 MHz frequency increments. This rather coarse scale causes the discontinuous jumps in power at the $f_{u,d}$ points in the figure to show up with finite slopes. The arrows indicate the direction of the frequency sweep which produced the specific response curves shown in each of the graphs. For graphs in Fig. 4(a) and (b), the double arrows and the R labels indicate that the response curves were more or less reversible. For graphs in Fig. (c) and (d), the arrows show the responses for increasing or decreasing frequencies, as indicated. The vertical dashed reference line at $f = 4170.3$ MHz shows the position of the f_{mo} resonance mode in the low power limit. The frequency parameters f_u and f_d denote the frequency jump points in graphs Fig. 4(b)–(d) associated with the up-sweep and down-sweep segments of the foldover response, respectively. For the graph in Fig. 4(b), these points coincide. There was no significant foldover for input powers of 0 dBm or lower.

The data in Fig. 4 show the typical foldover response first described by Weiss in 1958, and subsequently studied by numerous workers as summarized in the introduction. There are several noteworthy features of the data in Fig. 4. First, the four graphs trace the full evolution of the main mode MSW resonance from the low power response in Fig. 4(a), to the

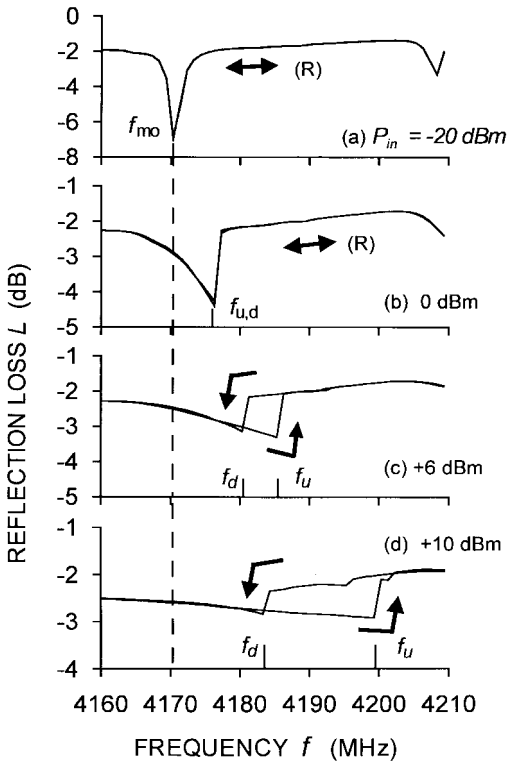

Fig. 4. Reflection loss L, in dB, as a function of frequency f for the resonator structure at various levels of CW input power $P_{\rm in}$, as indicated. The double arrows labeled R indicate reversible responses. The single arrows indicate the response for the indicated sweep direction. The vertical dashed line shows the position of the resonance peak absorption at 4170.3 MHz for the f_{mo} mode in the low power limit. The f_u and f_d frequency points indicate the up-sweep and down-sweep jump frequencies, respectively.

severely distorted but still reversible profile in Fig. 4(b), and then to the hysteretic foldover responses in Fig. 4(c) and (d).

Second, the general shift in the resonance is always toward higher frequency. This shift is directly related to the opening up of the precession cone angle of the magnetization as the power is increased, the corresponding decrease in the static component of the magnetization perpendicular to the film plane, and the resulting increase in the mode frequency from (2).

Third, there is a threshold power level for foldover. Graph (b) shows a severe distortion in the FMR absorption but no foldover. Graphs (c) and (d), on the other hand, exhibit clear foldover effects of the sort depicted schematically in Fig. 1. The power threshold for foldover will be an important consideration for the analysis to follow.

The overall foldover response will be considered in Section IV. However, in order to elucidate the nature of the response at the very outset, it is useful to consider the basic frequency shift with power shown by the data in Fig. 4. This effect can be made more evident by rewriting the mode frequency for $n = 1$ and $l = 1$ in the form

$$\frac{f_{1,1}}{|\gamma|} = (H_{\rm ext} + H_{adj}) - 4\pi M_z(P_a)\left(1 - \frac{2d}{a} - \frac{dk_{1,1}}{4}\right). \qquad (3)$$

The "(o)" frequency superscript in $f_{1,1}^{(o)}$, which denoted the low power limit, has now been removed and the saturation magnetization M_s has been replaced by its static component perpendicular to the film M_z. The P_a parameter in (3) denotes the power absorbed by the YIG film. The power dependent M_z factor is shown explicitly as $M_z(P_a)$ to emphasize the precession cone effect. The $2d/a$ and $dk_{1,1}/4$ terms are both well below unity. This means that the decrease in M_z with increasing P_a will result in a shift in the mode position to higher frequencies.

There is a clear upward shift in the frequency position of the main resonance peak from $f_{mo} = 4170.3$ MHz in the graph in Fig. 4(a) as the input power is increased. Careful measurements of this shift as the power is increased from -20 dBm to about -5 dBm, and before the strong asymmetry of the graph in Fig. 4(b) or the hysteresis evident in the graphs in Fig. 4(c) and (d) develop, give an initial frequency shift with input power β of about 8.5 MHz/mW. This response will be discussed in Section IV. Equation (2) gives a corresponding rate of decrease in $4\pi M_z$ of about 3 G/mW. If one assumes that the total magnetization M_s remains constant at the saturation value indicated above, the precession cone angle θ is connected to the z component of the magnetization through the condition $M_z = M_s \cos\theta$. For the values given above, the opening of the precession cone angle at an incident power of 1 mW, or 0 dBm, is on the order of a few degrees. This level of response for the onset of foldover is consistent with the results of Tsankov *et al.* in [18] for propagating MSFVW pulses in a YIG film delay line structure.

It will be shown below, however, that the foldover effects calculated solely on the basis of classical uniform mode precession cone and frequency shift arguments come in at lower powers and are much larger than the data show. These effects will be analyzed in Section IV.

Fig. 4 demonstrates the development of a foldover ferromagnetic resonance response for measurements of absorbed power versus frequency at a sequence of increasing power levels. Fig. 5 shows the same basic response, but for measurements of the reflected power versus incident power at a sequence of fixed operating point frequencies which are shifted by increasing amounts from the low power lowest order mode FMR frequency f_{mo}. Note the change in the horizontal input power scales from the graphs in Fig. 5(a) and (b) to the graphs in Fig. 5(c) and (d).

Fig. 5 shows that the frequency operating point f serves as a control parameter for bistability. As shown in the graph in Fig. 5(a), a relatively small $+1.5$ MHz shift in the operating point frequency from f_{mo} produces a small nonlinear notch in the power response but no bistability. Fig. 5(b)–(d) shows that larger frequency changes produce bistable response characteristics.

The bistable response develops for frequency operating points about 3 MHz above f_{mo}. The initial effect for operating points closer to f_{mo} is an increase in the steepness of the low power side of the nonlinear notch response shown in Fig. 5(a) and the development of a small but distinct downward jump in output power. This jump then separates into two jump points. As shown in Fig. 5(b)–(d), there is a jump to lower reflected powers when the input power is increasing, and a jump to higher reflected powers when the input power is decreasing.

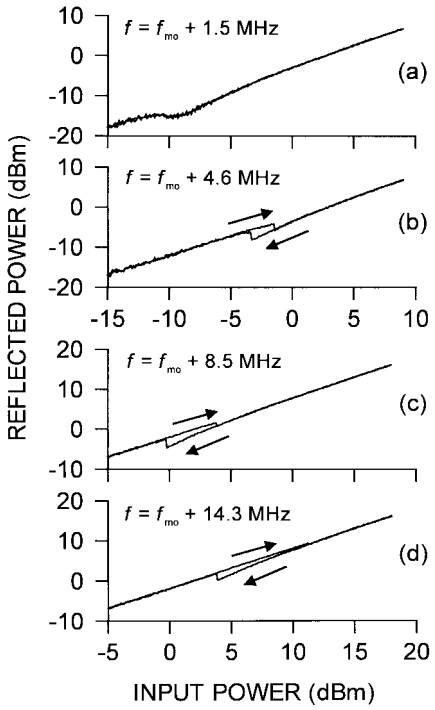

Fig. 5. Characteristic reflected power versus input power response curves for the YIG film resonator at different operating point frequencies relative to the low power main resonance frequency at $f_{mo} = 4170.3$ MHz. For the bistable response curves in (b)–(d), the arrows show the directions of the input power variation for the up-sweep and down-sweep segments of the response.

The size of the bistable output power response is small, on the order of 1–2 dB. As the frequency operating point moves away from f_{mo}, the bistable response shifts to higher input powers and the width of the bistable region also increases. Negative f shifts produced no nonlinear response characteristics.

C. Pulse Response

Measurements similar to those shown in Figs. 3–5 were also carried out under the pulse excitation conditions specified in Section II. The intent of these pulse measurements was to insure that sample heating was not an important consideration for the CW measurements. As noted in the introduction, sample heating can be an important consideration for FMR at high power levels for bulk ferrite samples with narrow linewidth, and such heating can sometimes produce a response which has the same appearance as foldover.

For an FMR linewidth of 2 MHz or so, as found for the low power FMR profile of Fig. 1(b), the response time for the FMR precession response is well below 1 μs. The relatively wide 1–10 μs pulses which were available for these measurements were sufficiently long, therefore, to achieve a near steady state FMR response. In combination with the 1 kHz repetition rate, these pulses give duty cycles in the 0.1–1% range. A duty cycle of one percent or smaller is sufficient to avoid heating effects in YIG film FMR [11], [13], [14]. The present pulse experiments provide access to the steady state FMR response and, at the same time, avoid heating effects.

As with the pulse measurements in [12]–[16], the use of pulses eliminated a foldover response. For the profile measurements versus frequency at different fixed input power levels, that is, pulse data which corresponded to the CW data in Fig. 4, the profiles obtained both for increasing frequency and for decreasing frequency were the same as the CW profiles for decreasing frequency. In other words, the profiles were identical for both frequency sweep directions and matched the down-sweep profiles in Fig. 4. The down-sweep distortions and jumps shown in Fig. 4 were reproduced, but hysteresis or foldover was not found.

The pulse measurements of peak output power versus input power profiles at fixed frequency, following the format of the CW data in Fig. 5, also showed no hysteresis or bistability character. The output power versus input power response profiles both for increasing input power and decreasing input power were identical. These profiles closely matched the CW power response profiles for increasing input power.

These pulse data confirm the conclusion of Seagle *et al.* [10] that the high power FMR response for small area YIG films is unrelated to heating effects. This follows from the experimental observation that the pulse data follow the frequency down-sweep and the increasing power profiles obtained with CW microwave power.

The match between the pulse data and the CW profiles for increasing input power at fixed frequency is physically reasonable. The application of each pulse corresponds to a turning on, or increase, of the microwave power. The match-up also confirms that 1–10 μs pulses are sufficient to achieve a steady state response. Other measurements on the 1 mm $\times$ 4 mm film for a wide range of pulse widths and instantaneous measurement times relative to the start of the pulse confirmed that pulses in the range from 2–100 μs yield a steady state response with no heating effects.

The match between the pulse data and the CW data for decreasing frequency at fixed power is consistent with the power profile results described above. If one assumes that each pulse acts independently and corresponds to a turn-on of the microwave power, one may easily take the data at some fixed power level from the increasing power response curves in Fig. 5 and construct the corresponding profiles one would obtain as a function of frequency. The frequency response profiles so constructed correspond to the down-sweep profiles in Fig. 4. The fact that the pulse data match the down-sweep frequency profiles is consistent, therefore, with the power profile results.

It is clear, however, that additional pulse measurements will likely provide important clues to the physical processes responsible for these foldover effects. The analysis of the next section will show that a classical precession model, in itself, cannot explain the foldover response, and that the frequency jumps on both up-sweep and down-sweep occur sooner than the model predicts. This implies that spin wave instability processes may be important, even for the perpendicular FMR configuration. As pointed out by Suhl in 1960 [4], if such processes were active, the jumps would occur sooner, and would therefore produce a foldover response which more closely matches the data.

A key test of the importance of Suhl processes would be to perform pulse measurements as a function of pulse width in the 100 ns to 1 μs range. While the FMR relaxation rate is on the order of hundreds of nanoseconds, the relaxation rate for the parametrically driven spin waves can be somewhat larger. This is related to the fact that typical spin wave linewidths are smaller than the ferromagnetic resonance linewidths for the same material. For just the right pulse width, one should see classical foldover without the complication of spin wave instability processes. Further comments on spin wave processes will be provided in the next section.

IV. Foldover Analysis

A. Classical Foldover Response

This section will review the basic tenets of the classical nonlinear precession analysis which leads to the foldover effects originally proposed in [2]. The simplest approach is to use a standard linear FMR response analysis as in [25] as a starting point. One can then evaluate the dynamic magnetization m response to a transverse microwave field, write M_z to lowest order as

$$M_z = M_s - \frac{|\mathbf{m}|^2}{2M_s} \tag{4}$$

and obtain operational equations for the $\mathbf{m}$-dependent FMR frequency shift and the nonlinear power response which results from this shift.

For the analysis, it is important to include both the dispersive, or in-phase, as well as the absorptive, or out-of-phase dynamic magnetization response to the applied microwave field. While the out-of-phase response is responsible for the FMR loss and the absorbed power, the in-phase response contributes significantly to $\mathbf{m}$, and hence to M_z and the corresponding frequency shift. From Figs. 3 and 4, it is clear that the shifted profiles are moved up in frequency from f_{mo} by amounts which exceed significantly the low power mode linewidth. This is one experimental indication that dispersive terms in the response are important.

The above analysis yields two operational equations, one for the resonance response and one for the shift in the resonance frequency with power. The resonance response takes the familiar Lorentzian form specified from the low power FMR response [25]. This response may be written in the form

$$P_a(f) = P_{\mathrm{in}} \frac{A}{\left\{1 + \left[(f - f_m) \Big/ \frac{\Delta f}{2}\right]^2\right\}}. \tag{5}$$

The A parameter represents the absorption coefficient $P_a(f_m)/P_{\mathrm{in}}$ at resonance. For the 5 dB or so change in reflection loss at resonance in Fig. 3, the A parameter is about 0.7 for the YIG film resonator structure described above. The resonance frequency f_m in (5) is taken to be the power dependent main mode frequency. The Δf parameter in (5) represents the width of the Lorentzian resonance response. From the data in Fig. 3, this width is 2 MHz. The frequency

f_m may be written as

$$f_m = f_{mo} + BP_a \tag{6}$$

where B is a power response coefficient.

In the limit of very low power, one may ignore the BP_a frequency shift term in (6). The main mode frequency f_m then goes over to f_{mo} and (5) becomes a simple Lorentzian. In this limit, one can adjust A and Δf to fit (5) to the data of Fig. 3(b). The solid points in Fig. 3(b) show such a fit based on the equation

$$L(f) = L_b + 10 \log \left[\frac{P_{\text{in}} - P_a(f)}{P_{\text{in}}} \right] \tag{7}$$

with $P_a(f)$ given by (5) and the numerical parameter values A = 0.66 and $\Delta f = 1$ MHz. The fit shown includes also a third parameter, reflection loss away from resonance, taken as $L_b = -1.9$ dB. As the fit shows, (5) provides a very good match to the low power main mode FMR response for $B = 0$.

At higher powers, the power dependent frequency shift introduced through (6) will serve first to shift and then distort the FMR response. Recall from Section III that the observed initial shift in the FMR peak with input power prior to the development of asymmetry or foldover was about $\beta = 8.5$ MHz/mW. The frequency shift term in (6) is in terms of the absorbed power P_a rather than the input power. This means that the B parameter should be of the order of $\beta/A = 8.5/0.66 \approx 13$ MHz/mW.

At higher powers, (5) and (6) may be solved to obtain response curves which are qualitatively similar to the schematic profile in Fig. 1 or the measured profiles in Figs. 4 and 5. One may also use (5) and (6) to evaluate frequency jump points for up-sweep and down-sweep frequency traces at fixed power or power jump points for increasing and decreasing power traces at fixed frequency. Such calculated profiles and jump points provide a quantitative way to compare theory with experiment, since the jump points may be measured explicitly from data of the sort shown in Figs. 4 and 5. Such comparisons will be shown at the end of this section.

B. Reduced Parameter Analysis

Although results from the classical foldover analysis based on the FMR response at large precession angles are shown in many of the references cited above, it will prove useful to summarize some of the basic response equations in a convenient reduced parameter format. The three experimental parameters are the frequency f, the input power P_{in}, and the absorbed power P_a. Useful reduced frequency, input power, and absorbed power parameters may be defined by

$$\phi = \frac{f - f_{mo}}{\Delta f/2} \tag{8}$$

$$g = \frac{ABP_{\text{in}}}{\Delta f/2} \tag{9}$$

and

$$W = \frac{BP_a}{\Delta f/2} \tag{10}$$

respectively. The numerators for these new parameters have units of frequency, and the common $\Delta f/2$ divisors produce dimensionless parameters with the frequency numerators scaled to the low power FMR linewidths.

In terms of these new parameters, the nonlinear FMR response based on (5) and (6) takes the form of a cubic equation given by

$$W^3 - 2\phi W^2 + (1 + \phi^2)W - g = 0. \tag{11}$$

For any given field and input power level, the roots for W as a function of frequency define the resonance response. Formally, the transition from a single valued absorption to a foldover response is related to the change in the number of unequal real roots to (11) from one to three. From the well-known root analysis for cubic equations, one may write $W = w + 2\phi/3$ and reduce (11) to the form $w^3 + aw + b = 0$, with the a and b parameters given by $a = 1 - \phi^2/3$ and $b = 2\phi^3/27 + 2\phi/3 - g$. The character of the roots to (11) is determined by the sign of the discriminant $D = 4a^3 + 27b^2$. For $D < 0$, there are three real roots. For $D > 0$, there is only one real root. For $D = 0$, two real roots exist if a and b are nonzero and there is only one real root if a and b are both zero. For $a = b = 0$, one obtains the power threshold for foldover at $g = g_{th} = 8\sqrt{3}/9$. For $g > g_{th}$, the $D = 0$ condition yields an explicit analytical relation between the two jump point frequencies and power.

Equation (11) may be solved explicitly for the frequency parameter ϕ

$$\phi = W \pm \sqrt{\frac{g}{W} - 1}. \tag{12}$$

Equation (12) provides an explicit analytical function for the response. For a given value of the input power P_{in}, and hence for a specific value of g, the maximum value of the reduced loss parameter W at the resonance peak is simply $W = W_{\text{res}} = g$ and the position of this peak is at $\phi = \phi_{\text{res}} = W_{\text{res}} = g$. If W is used as the control parameter and stepped down from the peak value at $W_{\text{res}} = g$ to zero, the $\pm$ signs in (12) serve to trace out the two sides of the nonlinear FMR response.

If the reduced power parameter g is sufficiently small, one obtains a near Lorentzian response profile for W versus ϕ, and the corresponding P_a versus f profile as well. As g is increased, the W versus ϕ profile first distorts and becomes asymmetric. When g exceeds $g_{th} = 8\sqrt{3}/9$, the W versus ϕ profile folds over and takes on the appearance shown in Fig. 1. High g values, therefore, lead to the hysteretic foldover response discussed above. From (9), this threshold value of g corresponds to a threshold power for foldover given by

$$P_{\text{in}}^{\text{thresh}} = \frac{8\sqrt{3}}{9} \frac{\Delta f/2}{AB}. \tag{13}$$

For the parameters given above, $P_{\text{in}}^{\text{thresh}}$ is 0.179 mW or -7.46 dBm. This result illustrates a critical failing of the simple classical precession model, a threshold for foldover which is well below the observed experimental power threshold for foldover. From the graph in Fig. 4(b), the resonance response at $P_{\text{in}} = 0$ dBm $= 1$ mW, while highly distorted, shows no foldover whatsoever.

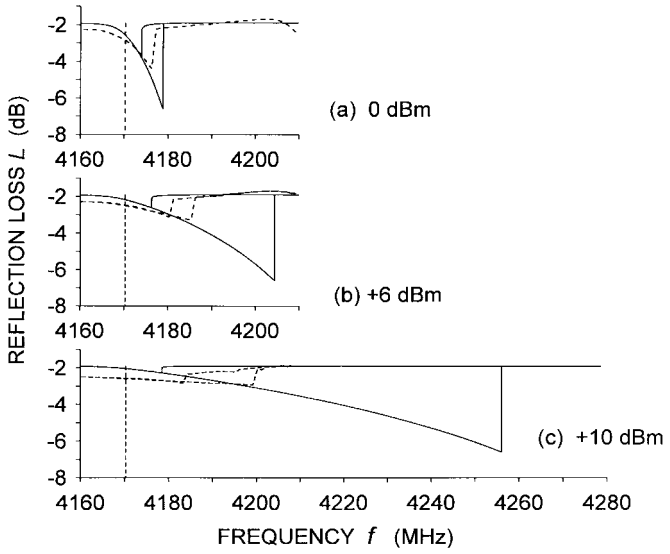

Fig. 6. Reflection loss L, in dB, as a function of frequency f for the resonator structure at various levels of CW input power $P_{\rm in}$ as indicated. The solid lines show the calculated foldover response based on fitted parameters to the data at -20 dBm input power. The dashed foldover response curves show the data from Fig. 4. The vertical dashed lines at $f = 4170.3$ MHz indicate the low power main FMR mode position. Directions of the frequency sweep are not shown, but correspond to those in Fig. 4.

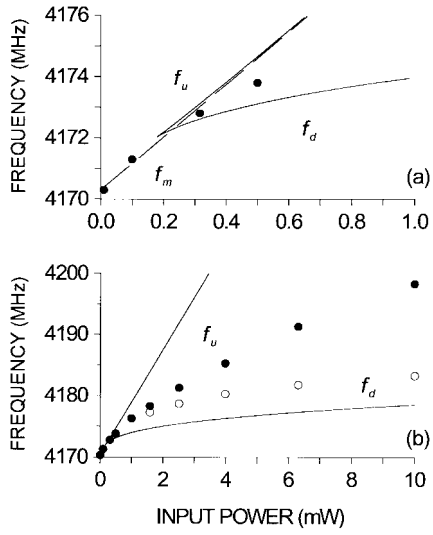

Fig. 7. Calculated and measured frequency jump points and shifts for the main mode profiles as a function of the input power. The solid lines show the calculated frequency jump points f_u and f_d based on the fitted parameters to the main mode profile at -20 dBm input power. The dashed line in graph (a) shows the shift in the main mode frequency f_m versus input power from (5) with $B = 13$ MHz/mW. The solid circles in graph (a) show the measured frequency shift for the main mode. In (b), the solid and open circles show the f_u and f_d jump point data, respectively.

For power levels above threshold, one may also solve (11) for the theoretical jump point frequencies f_u and f_d indicated in Fig. 1. From the W values at these jump frequencies from (13) and the profile solutions from (12), one may construct response profiles which correspond to the data in Fig. 4. These computed profiles and jump point frequencies will only be a function of the A, B, and Δf parameters used to fit the low power FMR response in Fig. 3 and the input power $P_{\rm in}$. These computed FMR profiles and jump point frequencies may then be compared with the results of the measurements.

C. Comparisons with Experiment

Fig. 6 shows comparisons of computed FMR profiles with the measurements shown in the graphs in Fig. 4(b)–(d) for input powers of 0, +6, and +10 dBm, as indicated. The computed profiles were based on the A, B, and Δf parameter values from the fit of the low power Lorentzian response of (6) to the data in Fig. 3(b). Conversion from reduced parameters to profiles of reflection loss versus frequency was made through (8)–(10). The format follows Fig. 4. The solid lines show the computed profiles and the dashed lines reproduce the experimental profiles from Fig. 4.

It is clear from the computed profiles in Fig. 6 and the overlay of the measured profiles on these results, that the classical FMR foldover model based on a linear shift in the FMR frequency with power falls far short of explaining the YIG film experimental results. Even the profiles at the lowest power shown, 0 dBm, reveal a basic discrepancy. The data at this power level show about the right overall shift, but exhibit no foldover. The computed profiles exhibit substantial foldover. As one moves to higher input powers, one finds a foldover response for both the calculated profiles and the data, but the actual profiles are very different. The computed high frequency up-sweep jump point frequency, for example, moves up substantially as the power is increased. At $P_{\rm in} = +6$ dBm, this jump point is 20 MHz above the experimental jump point. At $P_{\rm in} = +10$ dBm, this jump point is 55 MHz above the corresponding experimental jump point.

As will be discussed shortly, the calculated high frequency jump point response shown in Fig. 6 corresponds almost exactly to the mode frequency shift with power contained in (5), with the numerical B value of 13 MHz/mW which is obtained from the observed shift in the FMR peak position with power at very low powers. The large detuning which would be needed to produce the extremely large computed shifts and high frequency jump points in Fig. 6 would have to come from a substantial change in M_z in (4), and hence, from a very large dynamic response $\mathbf{m}$.

The data show, however, that such a large dynamic response is not realized experimentally. One possible explanation of the failure of the classical model is the parametric excitation of spin waves. Suhl suggested such a process many years ago [4] and produced computed response curves which showed foldover effects. Comments on Suhl processes are given below.

Fig. 7 shows comparisons between the computed frequency jump points as a function of the input power with the jump points found from the experimental profiles. Fig. 7(a) shows the computed response and the low power data points on an expanded scale. The solid lines in Fig. 7(a) show the computed jump point frequencies, based on the above mentioned condition $D = 0$. The dashed line shows the main mode peak frequency shift from (5) for $B = 13$ MHz/mW. Fig. 7(b) shows the computed and measured low and high frequency jump points as a function of the input power for $P_{\rm in}$ values out to 10 mW.

Fig. 7(a) shows three important results. First, the dashed line starts at the low power main mode frequency of 4170.3 MHz and extends upward through the first few data points. These are single data points for low power and no foldover which correspond only to the shift in the peak of the main mode position. The slope of the dashed line corresponds to the already cited value $\beta = BA \approx 8.5$ mW / Oe.

Second, the calculated jump frequency points have a common point of convergence at the power threshold for foldover, $P_{\rm in} = P_{\rm in}^{\rm thresh} = 0.179$ mW. The frequency at this common point corresponds to the frequency at which the main mode FMR profile has a vertical slope. For larger powers, the profile will fold over as shown schematically in Fig. 1. This frequency value is slightly above the linear main mode frequency versus power response line by about 0.1 MHz. This is because at the threshold for foldover, the position of the vertical slope region of the profile is slightly above the peak position.

Third, and this is the most interesting result from Fig. 7(a), as the input power increases from $P_{\rm in} = P_{\rm in}^{\rm thresh}$, the high frequency jump point rapidly merges with the dashed line main mode frequency shift response. One can see, therefore, that in the limit of high power, the high frequency jump point in the classical model simply corresponds to the power dependent frequency shift of the FMR peak.

Turn now to Fig. 7(b). As in Fig. 6, these results show the wide disparity between the predictions of the classical precession foldover model and the YIG film data. First, and as has been emphasized previously, the development of foldover actually occurs for input power levels somewhat above 1 mW. This is 7–8 dB higher than predicted by the precession model. Second, the calculated high frequency jump point frequency f_u increases linearly with $P_{\rm in}$ and moves well above the measured jump points. This major discrepancy is also apparent from the extended up-sweep part of the calculated profile shown in Fig. 6(c). Third, the calculated down-sweep jump point frequency f_d seems to be displaced down from the data by a relatively constant amount of 5 MHz or so.

From the results in Figs. 6 and 7, it is clear that the frequency jumps associated with foldover occur sooner on both the up-sweep and the down-sweep segments of the FMR profile. Some mechanism other than a simple shift in the main mode frequency with power because of a wider and wider classical precession cone must be responsible for these properties.

D. Possible Theoretical Directions

No attempt has been made to develop a new nonlinear theory for foldover. The beginning points for such a theory based on the parametric excitation of spin waves are contained in the brief comment by Suhl cited above [4] and the keynote papers on spin wave instability processes and the steady state response above threshold by Suhl [26] and Schlömann [27]. Such processes could, in effect, result in a more rapid decrease in the z component of the magnetization. The present results demonstrate clearly that the classical precession model does not account for the observed foldover response in high power FMR for perpendicular magnetized narrow linewidth YIG films. The pulse data presented above show that extraneous effects, such as heating, are not present. The frequency and power sweep data taken under pulse conditions also demonstrate that the measured effects represent a true foldover response for the steady state FMR signal. Further work is needed to clarify the possible effect of parametric spin waves for perpendicular FMR, quantify any possible foldover response driven by parametric spin waves, and make accurate comparisons with experiment in the same spirit as the comparisons in Fig. 6.

In the case of YIG film FMR with the static magnetic field in the plane of the film, Zhang *et al.* [11], [13] did show that low duty cycle pulsed measurements at high power lead to the characteristic resonance linebroadening which results from the parametric excitation of spin waves as predicted by Suhl [26]. In addition, Chen *et al.* [14] showed that the classical foldover analysis could explain such data only if the linewidth was forced to increase with power as is found for Suhl processes. In the case of in-plane static fields, however, one has spin waves at the FMR frequency which are available for such excitation. When the static field is perpendicular to the film plane, as in the present experiments, such spin waves are not available, and it is not clear how parametric spin wave processes could be operative to ameliorate the dynamic response.

It was not considered productive to embark on an involved fitting procedure based on additional power dependences for the A and Δf parameters in (5), nevertheless, a few simple numerical evaluations do indicate that an A parameter which decreases with increasing power and a Δf parameter which increases with power lend some improvement to the match between the calculations and experiment. Such changes are consistent with what one finds for resonance saturation due to Suhl parametric processes [11], [13], [14]. Additional terms in the power dependence of the main mode frequency in (6) also lend improvement to the calculated response.

Further pulse measurements could provide clues to the processes responsible for FMR foldover in YIG films. The pulse measurements described above were for low duty cycles, in order to avoid sample heating effects. The pulse widths were set at one microsecond and above to ensure that one was observing the steady state FMR response. It would be useful to make similar measurements for shorter pulses which extend below the typical microwave relaxation times of 100–500 ns or so for YIG films. If spin wave processes are important, it will also be important to consider the spin wave relaxation time. This relaxation time can be somewhat smaller than the FMR relaxation time under certain circumstances. In any event, one might project that measurements as a function of pulse width down to approximately 10–20 ns or so could serve to isolate spin wave processes, transient FMR response effects, and steady state precession considerations.

V. Comment on Applications

Apart from the unresolved theoretical issues, the above results make possible some comments about applications of a YIG film based bistable resonator for microwave signal processing. As shown in Fig. 5, the YIG film resonator can

provide a low or high power output state when operated in time bistable input power region. One could envision a device, for example, in which the resonator is switched from the low power to the high power state simply by the application of an additional microwave pulse of the right power. This means that the YIG film based bistable resonator could be used as a microwave modulator which is controlled directly by microwave power.

Microwave limiter applications are also possible. This could be accomplished, for example, through the dependence of the resonator frequency on power. This frequency could be tuned by the application of an additional microwave pulse and drive the response from a high loss state to a low loss state. An array of such devices could form the basis for microwave power logic.

One should note also that there are different ways to configure the resonator in microwave circuits. For the setup shown in Fig. 2, the resonator is configured as a rejection filter. As has been demonstrated, this configuration provides a difference between high and low reflected power levels of several dB. If this device was reconfigured as a passband filter, for example, it could provide a difference in the high and low level transmitted power states by 10 dB or more. In a passband configuration, the resonator could be used as a very efficient microwave power limiter.

VI. Summary

The microwave foldover and bistability response characteristics of a YIG film resonator have been examined experimentally and modeled in terms of the classical precession response. The resonator was configured as a rejection filter and utilized a narrow linewidth single crystal yttrium iron garnet film magnetized to saturation perpendicular to the film plane by an applied magnetic field which was held at a fixed value for all of the measurements. As a function of increasing microwave power, the frequency swept FMR profiles first distort and become highly asymmetric, and then develop a foldover characteristic which is qualitatively consistent with classical precession considerations. Profiles of output power versus input power at fixed frequency also exhibit a foldover or bistable response for frequencies somewhat above the lower power FMR frequency point. Pulse measurements were used to confirm that heating effects were not responsible for the observed effects and that *bona fide* foldover processes were obtained in the experiments. The foldover or bistable response amounted to a change in output power in the range of 1 dB, a hysteresis width in frequency up to 20 MHz at an input power of +10 dBm, and a hysteresis width in power of about 5 dB for an operating point frequency detuned from the low power FMR frequency by 14 MHz.

The low power FMR response could be accurately modeled in terms of a Lorentzian response function consistent with small signal theory. This parametrized response was used as the starting point in a classical precession model to calculate power thresholds for foldover, actual foldover profiles, and frequency jump points for the bistable responses which produce foldover. In accord with classical theory, the FMR frequency was taken to increase linearly with power. The results of these calculations were not in accordance with the measurements. First, the predicted power threshold for foldover was 7–8 dB lower than found experimentally. Second, the frequency width of the foldover regions far exceeded the widths found experimentally. At +10 dBm input power, for example, the calculated profile had a frequency width of 75 MHz, compared to the experimental width of less than 20 MHz. The high frequency up-sweep jump point was always well above the data. The low frequency down-sweep jump point was typically 4–5 MHz below the data.

Possible avenues for theoretical work are suggested. These include an examination of spin wave instability processes as an additional mechanism to produce a decrease in the z component of the static magnetization with increasing power and, hence, promote a foldover response more consistent with experiment. Potential problems with such a mechanism are also pointed out. Additional pulse measurements are suggested as a way to separate various contributions to the foldover response. Finally, a brief perspective on device applications of foldover and bistability in YIG film resonator structures is given. Possibilities include microwave modulators and limiters which are controlled directly through the application of microwave pulse signals. There are also possibilities for microwave logic.

Appendix
Definitions of Symbols and Acronyms

FMR	Ferromagnetic resonance.
MSW	Magnetostatic wave.
YIG	Yttrium iron garnet.
P_a	Absorbed power.
f	Frequency.
MSSW	Magnetostatic surface wave.
L	Reflection loss.
f_{mo}	Main resonance mode frequency.
f_{so}	Secondary resonance mode frequency.
MSFVW	Magnetostatic forward volume wave.
$k_{n,l}$	Allowed in-plane MSFVW wave numbers.
n, l	Integer mode indices.
a	Side length for square YIG film.
d	YIG film thickness.
$f_{n,l}^{(o)}$	Frequency of the (n, l) mode.
γ	Absolute value of the gyromagnetic ratio.
H_{ext}	Applied external static magnetic field.
H_{adj}	Adjustment field to account for anisotropy and other small neglected field terms.
$4\pi M_s$	YIG saturation induction.
k	Generic wave number.
$f_{1,1}^{(o)}$	Calculated MSFVW frequency for the main mode at low power.
$f_{1,3}^{(o)}$	Calculated MSFVW frequency for the secondary mode at low power.
P_{in}	Input power.
f_u, f_d	Frequency jump points associated with the up-sweep and down-sweep segments of the foldover response.

R	Reversible frequency sweep traces.
$f_{1,1}$	Main mode MSFVW frequency in terms of the z component of the magnetization.
β	Main mode frequency shift per unit change in input power.
M_z	Static magnetization z-component.
Θ	Precession cone angle for the main mode.
$\mathbf{m}$	Dynamic magnetization response.
A	Main mode absorption coefficient at resonance.
f_m	Power dependent main mode frequency.
Δf	Width at half power of the model main mode Lorentzian resonance response.
B	Main mode frequency shift per unit change in absorbed power.
L_b	Nominal return loss dB value off resonance.
ϕ	Reduced frequency parameter for foldover analysis.
g	Reduced input power for foldover analysis.
W	Reduced absorbed power parameter for foldover analysis.
w	Shifted cubic equation absorbed power parameter.
a	Shifted cubic equation linear term coefficient.
b	Shifted cubic equation constant term.
D	Cubic equation discriminant.
$g_{\rm th}$	Threshold value of reduced input power parameter g for foldover.
$W_{\rm res}$	Value of W at the main mode resonance peak.
$\phi_{\rm res}$	Value of ϕ for the main mode resonance peak.
$P_{\rm in}^{\rm thresh}$	Theoretical threshold power for foldover for the classical precession model.

ACKNOWLEDGMENT

The YIG film sample was provided by Dr. J. D. Adam of the Northrop Grumman Research and Development Laboratories, Pittsburgh, PA. Dr. C. Mathieu is acknowledged for a careful reading of the manuscript.

REFERENCES

[1] H. M. Gibbs, *Optical Bistability: Controlling Light with Light.* New York: Academic, 1985.
[2] P. W. Anderson and H. Suhl, "Instability in the motion of ferromagnets at high microwave power levels," *Phys. Rev.*, vol. 100, pp. 1788–1789, 1955.
[3] M. T. Weiss, "Microwave and low-frequency oscillation due to resonance instabilities in ferrites," *Phys. Rev. Lett.*, vol. 1, no. 7, pp. 239–241, 1958.
[4] H. Suhl, "Foldover effects caused by spin wave interactions in ferromagnetic resonance," *J. Appl. Phys.*, vol. 31, no. 5, pp. 935–936, 1960.
[5] P. Gottlieb, "Nonlinear effects of crystalline anisotropy on ferrimagnetic resonance," *J. Appl. Phys.*, vol. 31, no. 11, pp. 2059–2062, 1960.
[6] J. I. Masters, "Instability of magnetic resonance in single crystal spheres of yttrium iron garnet," *J. Appl. Phys.*, vol. 31, pp. 41S–42S, 1960.
[7] I. B. Goldberg, "Low power nonlinear effects in the ferromagnetic resonance of spheres of $Ba_3Zn_2Fe_{24}O_{41}$," *J. Appl. Phys.*, vol. 51, no. 3, pp. 1857–1859, 1980.
[8] L. M. Silber, C. E. Patton, and H. F. Naqvi, "Low power nonlinear effects in the ferromagnetic resonance of Zn_2 Y and MnZnY hexagonal ferrites," *J. Appl. Phys.*, vol. 54, no. 7, pp. 4071–4075, 1983.
[9] K. D. McKinstry, C. E. Patton, and M. Kogekar, "Low power nonlinear effects in the ferromagnetic resonance of yttrium iron garnet," *J. Appl. Phys.*, vol. 58, no. 2, pp. 925–929, 1985.
[10] D. J. Seagle, S. H. Charap, and J. O. Artman, "Foldover in YIG," *J. Appl. Phys.*, vol. 57, no. 1, pp. 3706–3708, 1985.
[11] Y. T. Zhang, C. E. Patton, and M. V. Kogekar, "Ferromagnetic resonance foldover in single crystal YIG films—Sample heating or Suhl instability," *IEEE Trans. Magn.*, vol. 22, pp. 993–995, Sept. 1986.
[12] K. Gnatzig, H. Dötsch, and A. Brockmeyer, "Ferrimagnetic resonance in garnet films at large precession angles," *J. Appl. Phys.*, vol. 62, no. 12, pp. 4839–4843, 1987.
[13] Y. T. Zhang, C. E. Patton, and G. Srinivasan, "The second-order spin-wave instability threshold in single-crystal yttrium iron garnet films under perpendicular pumping," *J. Appl. Phys.*, vol. 63, no. 11, pp. 5433–5438, 1988.
[14] M. Chen, C. E. Patton, G. Srinivasan, and Y. T. Yang, "Ferromagnetic resonance foldover and spin-wave instability in single-crystal YIG films," *IEEE Trans. Magn.*, vol. 25, pp. 3485–3487, Sept. 1989.
[15] M. Lührmann, M. Ye, H. Dötsch, and A. Gerspach, "Nonlinearities in the ferrimagnetic resonance in epitaxial garnet films," *J. Magnetism Magn. Mater.*, vol. 96, no. 1–3, pp. 237–244, 1991.
[16] N. Bahlmann, R. Gerhardt, M. Wallenhorst, and H. Dötsch, "Determination of the ferrimagnetic precession cone of in-plane magnetized garnet films using optical modulation technique," *J. Appl. Phys.*, vol. 80, no. 7, pp. 3977–3981, 1996.
[17] H. Yan, Q. Wang, and I. Awai, "Resonant frequency shift in a MSSW-SER with excitation power," *Electron. Lett.*, vol. 32, pp. 1787–1789, 1996.
[18] M. A. Tsankov, M. Chen, and C. E. Patton, "Magnetostatic wave dynamic magnetization response in yttrium iron garnet films," *J. Appl. Phys.*, vol. 79, no. 3, pp. 1595–1603, 1996.
[19] W. Shiltz, "Spin-wave propagation in epitaxial YIG films," *Philips Res. Rep.*, vol. 28, no. 1, pp. 50–61, 1973.
[20] A. D. Boardman, S. A. Nikitov and Q. Wang, "Theory of bistable magnetostatic surface waves," *IEEE Trans. Magn*. vol. 30, pp. 1-13, Jan. 1994.
[21] Y. K. Fetisov, P. Kabos and C. E. Patton, "Bistable microwave oscillator with magnetostatic wave signal-to-noise enhancer in the feedback loop," *Electron. Lett*., vol. 32, no. 20, pp. 1894-1895, 1996.
[22] Y. K. Fetisov and C. E. Patton "Microwave bistability in a magnetostatic surface wave interferometer with external feedback," *IEEE Trans. Magn*., vol. 35, pp.1024-1036, Mar. 1999.
[23] R. W. Damon and H. van de Vaart, "Propagation of magnetostatic spin waves at microwave frequencies in a normally-magnetized disk," *J. Appl. Phys*., vol. 36, no. 11, pp. 3453-3459, 1965.
[24] R. J. Joseph and E. Schlmann, "Demagnetizing fields of nonellipsoidal bodies," *J. Appl. Phys*., vol. 36, pp. 1579-1593, 1965.
[25] B. Lax and K. J. Button, Microwave Ferrites and Ferrimagnetics, McGraw-Hill, New York, 1962.
[26] H. Suhl, "The theory of ferromagnetic resonance at high signal power levels," *J. Phys. Chem. Solids*, vol. 1, pp. 209–227, 1957.
[27] E. Schlömann, "Ferromagnetic resonance at high power levels," Raytheon Tech. Rep. R-48, 1959, unpublished.